ISOMAse
International Society of Ocean, Mechanical and Aerospace Scientists and Engineers

Journal of Ocean, Mechanical and Aerospace
-Science and Engineering-
30 March 2026. Vol.70 No.1

DOI:
10.36842/jomase.v70i1.592

Resistance Analysis of a Fishing Vessel with a Dihedral Bulbous Bow and Retractable Bow Foil Variations

Muhammad Al Jabbar [a] and Fajri Ashfi Rayhan [a*]

[a)]*Department of Naval Engineering, Faculty of Engineering, University of Pembangunan Nasional Veteran Jakarta, Indonesia*

*Corresponding author: fajri.ar@upnvj.ac.id

Paper History

Received: 05-March-2026
Received in revised form: 19-March-2026
Accepted: 30-March-2026

ABSTRACT

Optimizing fishing vessel hull design is crucial for improving energy efficiency and meeting stringent environmental regulations. This study investigates the hydrodynamic resistance of a fishing vessel equipped with a dihedral bulbous bow and retractable bow foils, NACA 0015 and NACA 2408. Computational Fluid Dynamics (CFD) simulations based on Reynolds-Averaged Navier-Stokes (RANS) equations were conducted in calm water conditions. Contrary to the targeted resistance reduction, the baseline hull without foils exhibited the lowest total resistance across all tested velocities, recording 9.78 N at 1,286 m/s. Integrating the retractable foils increased total resistance by 27.48% (NACA 0015) and 15.23% (NACA 2408). This resistance penalty stems from an expanded wetted surface area amplifying frictional resistance, combined with interference resistance that disrupts the bulbous bow's streamline flow. Ultimately, the objective of a ≥10% resistance reduction was unachieved, establishing the unmodified baseline hull as the most hydro-dynamically efficient configuration.

KEYWORDS: *Computational Fluid Dynamics, Dihedral Bulbous Bow, Fishing Vessel, Retractable Bow Foil, Ship Resistance.*

NOMENCLATURE

L	Ship total length
B	Ship beam
D	Ship depth
∇	Volumetric displacement of ship
S	Wetted surface area
C_B	Block coefficient
C_P	Prismatic Coefficient
Fr	Froude number
g	Gravitational constant
R_t	Total resistance
R_v	Viscous resistance
R_P	Pressure resistance
C_P	Pressure coefficient
C_V	Viscous coefficient

1. INTRODUCTION

Substantial hydrodynamic resistance necessitates increased engine power to maintain a specified speed, which consequently elevates fuel consumption [1]. Therefore, optimizing ship design is a critical factor in mitigating this resistance and reducing the vessel's overall energy demands. The design of fishing vessels presents a uniquely complex challenge, as their operational profiles require varied service speeds corresponding to distinct activities, transiting to fishing grounds, searching for catch, conducting active fishing operations, and returning to port. Furthermore, these operational requirements must be balanced against increasingly stringent environmental regulations governing power and propulsion choices to minimize ecological impacts [2]. In 2011, concurrent with global efforts to address marine greenhouse gas emissions, the International Maritime Organization (IMO) implemented mandatory energy efficiency frameworks under MARPOL Annex VI [3]. These regulatory instruments established the Energy Efficiency Design Index (EEDI) for newly constructed vessels and the Ship Energy Efficiency Management Plan (SEEMP) for the existing global fleet.

Recent studies have extensively explored various computational and geometric optimization techniques to minimize hydrodynamic resistance in fishing vessels. For instance, Ali et al utilized Reynolds-Averaged Navier-Stokes (RANS) based Computational Fluid Dynamics (CFD) to evaluate two fishing vessel models, demonstrating that an optimized bulbous bow effectively mitigates resistance [4].

JOMAse | Received: 05 March-2026 | Accepted: 30-March-2026 | [(70) 1: 64-71]
Published by International Society of Ocean, Mechanical and Aerospace Scientists and Engineers, www.isomase.org., ISSN: 2354-7065 & e-ISSN: 2527-6085

ISOMAse
International Society of Ocean, Mechanical and Aerospace Scientists and Engineers
Journal of Ocean, Mechanical and Aerospace
-Science and Engineering-
30 March 2026. Vol.70 No.1
DOI: 10.36842/jomase.v70i1.592

Similarly, Lin et al investigated the implementation of a twin skeg hull configuration, which yielded an average reduction in total resistance of 5,4% compared to the baseline design [5]. Further geometric modifications were examined by Yu et al,who demonstrated that increasing the chine width and deadrise angle, alongside stern appendages, reduced total resistance by 2.36% [6]. Additionally, Iqbal et al applied targeted hull form optimization to small fishing vessels, achieving an average resistance reduction of 4.15% [7]. Collectively, these findings underscore that applying targeted geometric optimization can significantly diminish hydrodynamic resistance and enhance overall vessel efficiency.

Recent studies have investigated targeted structural modifications to optimize vessel efficiency. Díaz-Ojeda at all examined the impact of a dihedral bulbous bow on the hydrodynamic resistance of small fishing vessels [8]. Employing the CFD simulations and experimental towing tank tests, the Authors evaluated displacement and semi-displacement hull forms. Their findings demonstrated that integrating a dihedral bulbous bow can reduce total resistance by over 10% at specific velocities. Notably, this modification yielded greater efficacy on displacement hulls, primarily due to more pronounced and favorable alternations in the pressure distribution. Despite these significant resistance reductions, the scope for further hydrodynamic optimization remains broad. Exploring alternative appendages, Bockmann et al investigated the application of a retractable bow foil utilizing a NACA 0015 profile on a general cargo vessel [9]. While their results confirmed substantial decreases in hydrodynamic resistance and corresponding improvements in fuel efficiency, the implementation and analysis of retractable bow foils on fishing vessels remain largely unexplored in the current literature.

National Advisory Committee for Aeronautics (NACA) foil profiles are frequently implemented to enhance the hydrodynamic performance of marine vessels [10]. Specifically, the integration of NACA 0015 and NACA 2408 profiles facilitates superior hydrodynamic efficiency by optimizing the localized pressure distribution along the hull [11]. Demonstrating this potential, Chrismianto et al utilized CFD to investigate the installation of a NACA 2408 based hull vane on a 30 GT fishing vessel [12]. Their findings indicated a substantial total resistance reduction of up to 51,53% relative to the bare hull configuration. Building upon these established optimization strategies, the present study aims to analyze the hydrodynamic resistance of a fishing vessel equipped with a dihedral bulbous bow and retractable bow foil variations. Specifically, this research employs a CFD approach to analyze the impact of integrating retractable bow foils featuring both NACA 0015 and NACA 2408 profiles.

2. THEORETICAL BACKGROUND

Hull resistance refers to the hydrodynamic force that opposes a vessel's forward motion through water, thereby influencing operational efficiency and contributing directly to fuel consumption. According to Birk, the resistance experienced by a ship is influenced by the ship's speed, the weight of water displaced by the submerged part of the ship, and the design of the ship's hull [13].

In general, ship resistance is expressed as RT, which refers to total resistance, and can be explained by the following equation:

$$R_t = \frac{1}{2} . C_T . \rho . s . Vs^2 \quad (1)$$

Where R_t denotes the ship's total resistance (N), C_T is the dimensionless total resistance coefficient (-), represents the fluid density (kg/m³), s is the wetted surface area of the hull (m^2), and Vs is the ship speed (m/s).

Assessing the pressure distribution over the hull surface is essential for interpreting how variations in bulbous bow geometry influence overall hydrodynamic performance. In this context, the surface pressure coefficient, (C_P) is commonly employed to quantify local pressure intensity and is defined as follows:

$$C_P = \frac{P_H}{0.5\rho U^2 S} \quad (2)$$

Where P_H denotes the local pressure on the hull surface, is the fluid density,Urepresents the flow velocity, and S is the ship's wetted surface area.

The viscous resistance coefficient is systematically employed to quantify the combined impact of surface friction and form-induced drag. This coefficient is defined by the following equation:

$$C_V = (1 + k) . C_F \quad (3)$$

Where $C_F$represents the frictional resistance coefficient and k denotes the form factor (shape factor). This formulation allows for a precise evaluation of how geometric variations in the bow region modify the boundary layer development and, consequently, the total viscous energy loss.

The Froude number is a dimensionless parameter used to characterize free surface flows by comparing inertial effects to gravitational effects. It is expressed as follows:

$$Fr = \frac{Vs}{\sqrt{gL}} \quad (4)$$

Where Fr denotes the dimensionless Froude number (-), Vs is the ship speed (m/s), g is the gravitational acceleration (m/s^2), and L is the length between perpendiculars (m).

To simulate the complex turbulent flow field around the hull, the RANS equations are employed as the governing mathematical framework [14]. The steady-state momentum conservation for an incompressible Newtonian fluid is expressed as follows:

$$\rho \bar{u}_j \left(\frac{\partial \bar{u}_i}{\partial x_j}\right) = \rho \bar{f}_i + \frac{\partial}{\partial x_j}\left[- \bar{p}\delta_{ij} + \mu \left(\frac{\partial \bar{u}_i}{\partial x_j} + \frac{\partial \bar{u}_j}{\partial x_i}\right) - \rho \overline{u'_i u'_j}\right] \quad (5)$$

In this formulation, ρrepresents the fluid density,$\overline{u}$ denotes the time-averaged velocity components, and $\overline{p}$ is the mean pressure. The term $\rho \bar{f}_i$ accounts for external body forces, while μ represents the dynamic viscosity. The influence of turbulence is captured through the Reynolds stress tensor,$-\rho \overline{u'_i u'_j}$, which represents the fluctuating velocity components. To achieve closure of the RANS equations, this tensor is modelled using the$\kappa - \omega$ Shear Stress

JOMAse | Received: 05 March-2026 | Accepted: 30-March-2026 | [(70) 1: 64-71]
Published by International Society of Ocean, Mechanical and Aerospace Scientists and Engineers, www.isomase.org., ISSN: 2354-7065 & e-ISSN: 2527-6085

ISOMAse
International Society of Ocean, Mechanical and Aerospace Scientists and Engineers
Journal of Ocean, Mechanical and Aerospace
-Science and Engineering-
30 March 2026. Vol.70 No.1
DOI: 10.36842/jomase.v70i1.592

Transport (SST) turbulence model. This specific model is selected for its superior capability in blending the robust near wall formulation of the$\kappa - \omega$ model with the free-stream independence of the$\kappa - \epsilon$model, thereby accurately predicting adverse pressure gradients and flow separation around the ship's bulbous bow and foil appendages [15].

3. METHODS

The dihedral bulbous bow is an advanced iteration of the conventional bulbous bow, explicitly engineered to minimize hydrodynamic resistance and engine power consumption in small vessels. Constructed using developable surfaces, this was the geometric configuration optimizes propulsive efficiency. Consequently, it is particularly advantageous for vessels operating in displacement or semi-displacement modes, effectively mitigating wave-making resistance and enhancing overall hydrodynamic performance [16].

The Food and Agriculture Organization (FAO) of the United Nations provided a standard fishing vessel design to support the global fisheries sector, particularly within developing nations [17]. Accordingly, this study utilized the FAO1b model as the base model for the vessel resistance analysis. This specific hull was reconstructed based on [8]. To clearly distinguish the study model from the original reference and to maintain terminological consistency, the reconstructed hull was designated as FAO1b-PS (Present Study). In Figure 1 shows the FAO1b-PS lines plan. The principal dimensions derived from this design were established as shown in Table 1.

Table 1: Ship model main dimension

Dimensions	Value
L (m)	2.308
B (m)	0.751
D (m)	0.643
∇ (m^3)	0.103
S (m^2)	1.588
C_B	0.275
C_P	0.578

Following the initial modeling of the hull with a dihedral bulbous bow, subsequent design variations were developed to integrate a retractable bow foil system. This hydrodynamic appendage was installed at the bow and featured a mechanism enabling its deployment or retraction according to operational requirements. Such adaptability was identified as a critical factor in sustaining the vessel's efficiency across diverse sea states [18].

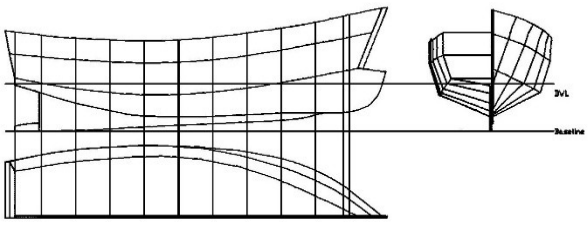

Figure 1: FAO1b-PS Lines plan

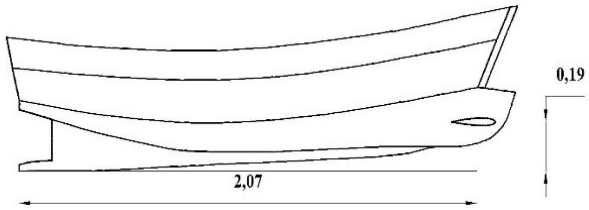

Figure 2: Side profile of the FAO1b-PS model and foil placement

The present study utilized two distinct foil profiles, NACA 0015 (Figure 3) and NACA 2408 (Figure 4). The geometric specifications for both appendages were standardized to a chord length of 0.2 m and a span of 0.4 m. These specific dimensions were selected to ensure an adequate projected area for evaluating the impact of the induced lift and resistance on the overall hydrodynamic performance of the vessel. As depicted in Figure 2, to ensure computational reproducibility, the precise installation position of the foils was established at a longitudinal distance of 2.07 m forward of the Aft Perpendicular (AP) and a vertical clearance of 0.19 m from the baseline. Furthermore, both foil configurations were mounted with an Angle of Attack (AoA) of 0°. This neutral angle was deliberately selected to align the appendages with the undisturbed incoming flow, thereby minimizing excessive form drag and isolating the fundamental hydrodynamic interference effects between the foils and the hull.

Figure 3: FAO1b-PS-0015

Figure 4: FAO1b-PS-2408

To analyze the fluid flow characteristics surrounding the investigated model, numerical simulations were executed utilizing ANSYS Fluent software. The computational domain and associated boundary conditions were established in accordance with the methodology outlined in a prior study [8]. Consequently, the specific spatial dimensions of the computational domain were defined in Table 2.

Table 2: Domain dimensions

Dimensions	Value
Domain length	16.0 m
Domain width	9.8 m
Domain height	4.6 m
Water depth	7.0 m

JOMAse | Received: 05 March-2026 | Accepted: 30-March-2026 | [(70) 1: 64-71]
Published by International Society of Ocean, Mechanical and Aerospace Scientists and Engineers, www.isomase.org., ISSN: 2354-7065 & e-ISSN: 2527-6085

ISOMAse
International Society of Ocean, Mechanical and Aerospace Scientists and Engineers
Journal of Ocean, Mechanical and Aerospace
-Science and Engineering-
30 March 2026. Vol.70 No.1
DOI: 10.36842/jomase.v70i1.592

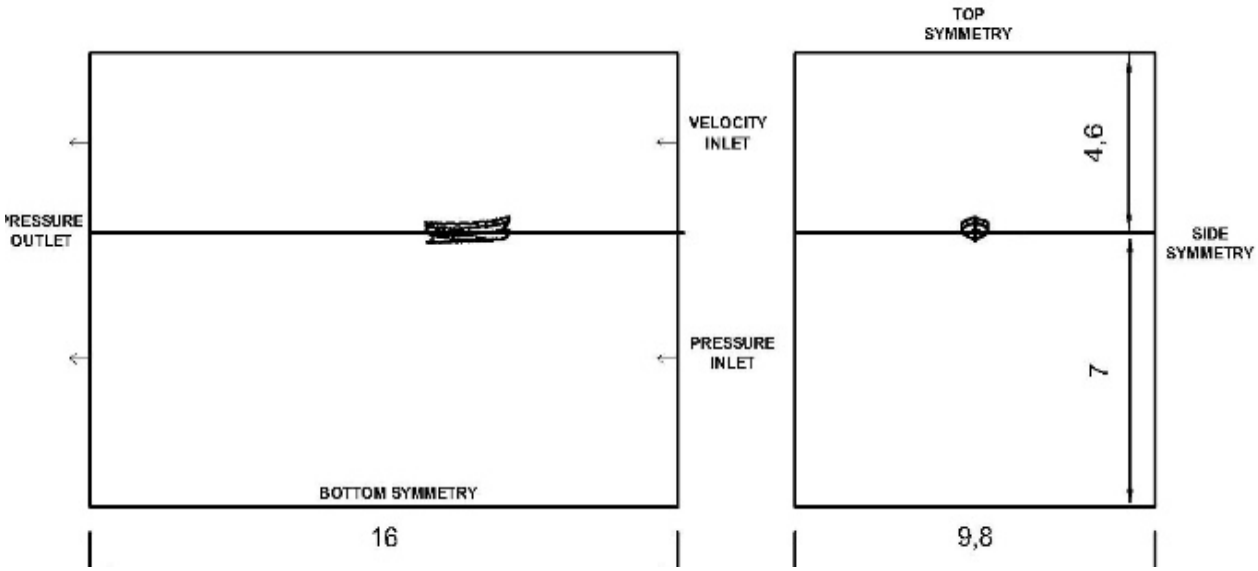

Figure 5: Boundary condition

Figure 5 and Table 2 presents detail of the computational domain and its boundary conditions. For the upstream boundary, a Velocity Inlet was assigned to the air phase and a Pressure Inlet to the water phase. The downstream boundary was set as a Pressure Outlet. To prevent far-field interference, Symmetry conditions were applied to the top, bottom, and side boundaries. Finally, the ship hull and foil appendages were defined as No-Slip Walls.

For the spatial discretization of the computational domain, a polyhedral meshing strategy was employed. The overall grid quality was strictly monitored using the orthogonal quality metric, and the maximum aspect ratio was maintained within permissible limits to ensure numerical stability in the steady-state turbulent flow simulations. To guarantee that the numerical results were independent of the grid size, a rigorous mesh sensitivity analysis was conducted. Three distinct grid configurations were evaluated: coarse (1.4 million elements), medium (1.9 million elements), and fine (2.2 million elements).

As presented in Table 3, the total resistance was monitored across these variations, demonstrating that the value converged as the grid density increased. Notably, the relative difference in total resistance between the medium and fine grids was negligible (approximately 0.06%). Consequently, the fine grid configuration comprising approximately 2.2 million cells was selected as the standard mesh for all subsequent analyses. In the final configuration, local sizing controls were applied, restricting the minimum cell size to 0.01 m to accurately capture the complex flow phenomena.

Table 3: Mesh convergence

Grid Density	Number of elements	Total Resistance (N)	Relative Difference (%)
Coarse	1.400.000	5.63	-
Medium	1.900.000	5.35	4.94%
Fine	2.200.000	5,36	0.06%

A three-dimensional (3D) numerical flow analysis was conducted utilizing the commercial CFD software, ANSYS Fluent. The numerical solver was based on the fundamental Reynolds-Averaged Navier-Stokes (RANS) equations to govern the incompressible, turbulent flow field around the hull. The free surface phenomenon between the water and air phases in calm water conditions was explicitly resolved by applying the Volume of Fluid (VOF) approach. For this multiphase formulation, the fluid densities were specified as 999.35 kg/m³ for the water and 1.0 kg/m³ for air.

Furthermore, the $k-\omega$ Shear Stress Transport (SST) turbulence model was employed to accurately capture the boundary layer and complex turbulence characteristics in the vicinity of the ship hull. This specific model was selected due to its well-documented superiority in predicting flow separation and handling adverse pressure gradients, which was highly critical for flows around complex geometric appendages such as the bulbous bow and the NACA foils. By effectively blending the robust near-wall formulation of the $k-\omega$model with the free stream independence of the $k-\epsilon$model, the SST formulation ensured a highly accurate computation of the viscous resistance. To maximize the accuracy of the near-wall formulation, the computational grid was carefully generated utilizing 10 inflation layers around the solid boundaries. This meshing strategy successfully resulted in an area-weighted average y^+ value of 4.27 for the general ship hull boundary and 36.42 for the submerged hull boundary. These values demonstrated that the grid resolution effectively leveraged the y^+insensitive wall treatment of the $k-\omega$SST model to capture the boundary layer development across the wetted surface area accurately.

The governing equations were solved utilizing a coupled pressure velocity algorithm, alongside a second-order upwind scheme for spatial discretization. This numerical configuration was implemented to guarantee high computational accuracy and robust convergence stability when predicting the hydrodynamic forces acting upon the ship model.

JOMAse | Received: 05 March-2026 | Accepted: 30-March-2026 | [(70) 1: 64-71]
Published by International Society of Ocean, Mechanical and Aerospace Scientists and Engineers, www.isomase.org., ISSN: 2354-7065 & e-ISSN: 2527-6085

ISOMAse
International Society of Ocean, Mechanical and Aerospace Scientists and Engineers
Journal of Ocean, Mechanical and Aerospace
-Science and Engineering-
30 March 2026. Vol.70 No.1
DOI: 10.36842/jomase.v70i1.592

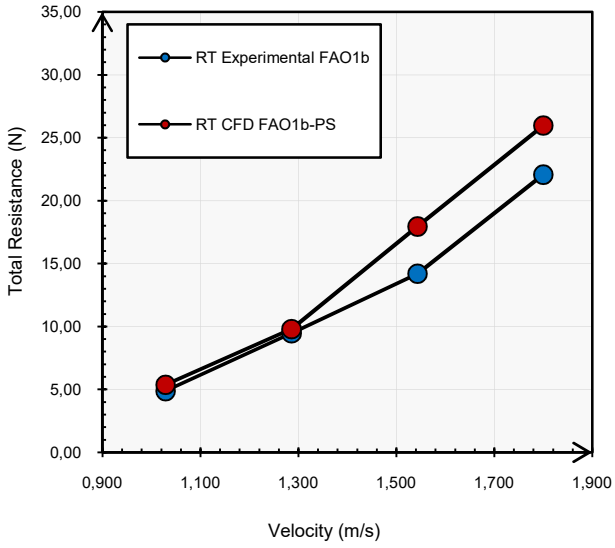

Figure 6: Model validation

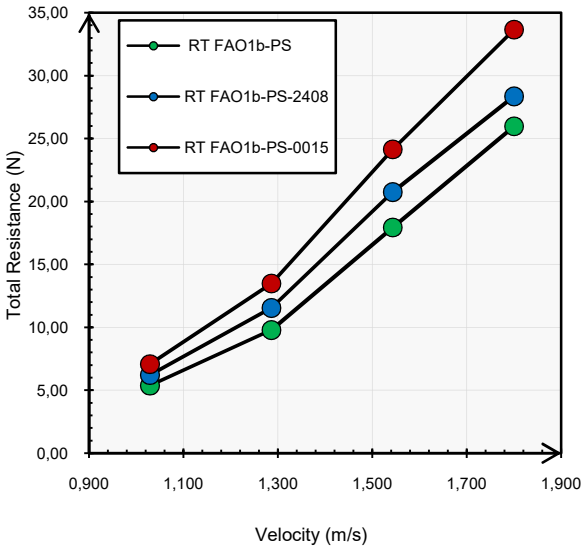

Figure 7: Total resistance

To ensure the reliability and accuracy of the CFD simulations prior to subsequent analyses, a rigorous numerical model validation was conducted. This validation process compared the total resistance values derived from the FAO1b-PS model simulations against the experimental baseline data of the FAO1b model, as reported in previous research [8].The validation procedure encompassed four distinct test velocities1.028, 1.286, 1.543, and 1.800 m/s, which corresponded to the vessel's operational range. This comparative analysis was conducted to assess the capability of the numerical model in accurately resolving the hydrodynamic characteristics and complex flow patterns developing around the hull.

As illustrated in Figure 6, the simulated FAO1b-PS model exhibited an increasing trend in total resistance that closely aligned with the FAO1b experimental data across the evaluated velocity range. Although deviations in the absolute values were observed with the CFD results consistently over-predicting the resistance, the minimum percentage deviation between the experimental and numerical data was recorded at 3.3%. This discrepancy did not alter the fundamental correlation between vessel speed and resistance. The strong conformity of this overall trend confirmed that the numerical setup adequately captured the physical flow phenomena, thereby establishing its validity and reliability for subsequent hydrodynamic analyses.

4. RESULT AND DISCUSSION

4.1 Total Resistance

Figure 7 illustrates the total resistance characteristics of the original FAO1b-PS ship model alongside two modified configurations equipped with NACA 0015 and NACA 2408 retractable bow foils. The computational results indicate that the baseline FAO1b-PS configuration yields the most favourable hydrodynamic performance, exhibiting the minimum total resistance across all evaluated speeds. For instance, at a velocity of 1,286 m/s, the baseline hull experiences a total resistance of 9.78 N, whereas the integration of the NACA 2408 and NACA 0015 foils increases the total resistance by 15.23% and 27.48%, respectively.

The observed increase in total resistance for the modified models can be attributed to alterations in both frictional resistance. Inherently, the integration of foil structures expands the vessels' Wetted Surface Area (WSA). According to fundamental hydrodynamic principles, this expansion in WSA leads to a proportional increase in frictional resistance, a component that heavily dominates at low to medium velocities where viscous effects govern the flow.

Furthermore, as demonstrated by [8], the efficacy of a bulbous bow relies heavily on its streamlined interaction with the surrounding fluid to mitigate wave generation. In the modified configurations, the appended foils introduce hydrodynamic interference that disrupts the streamline flow around the bulbous bow, thereby degrading the optimal wave cancellation effects inherent to the baseline design.

4.2 Viscous Resistance

As illustrated in Figure 8, the viscous resistance for all three model configurations exhibits a progressive increase with rising velocity. However, distinct performance disparities are evident among the designs. The baseline FAO1b-PS model consistently registers the lowest viscous resistance, whereas the integration of retractable bow foils elevates viscous resistance across the entire tested velocity spectrum. Between the modified variants, the FAO1b-PS-0015 configuration produces the highest viscous resistance, followed by the FAO1b-PS-2408.

This trend highlights the direct impact of the retractable bow foils on boundary layer development. By increasing the total WSA, the submerged appendages expand the area susceptible to fluid friction. Because viscous resistance originates from sheer stresses generated by the fluid surface velocity differentials, any addition of WSA fundamentally heightens this resistance component.

JOMAse | Received: 05 March-2026 | Accepted: 30-March-2026 | [(70) 1: 64-71]
Published by International Society of Ocean, Mechanical and Aerospace Scientists and Engineers, www.isomase.org., ISSN: 2354-7065 & e-ISSN: 2527-6085

ISOMAse
International Society of Ocean, Mechanical and Aerospace Scientists and Engineers
Journal of Ocean, Mechanical and Aerospace
-Science and Engineering-
30 March 2026. Vol.70 No.1
DOI: 10.36842/jomase.v70i1.592

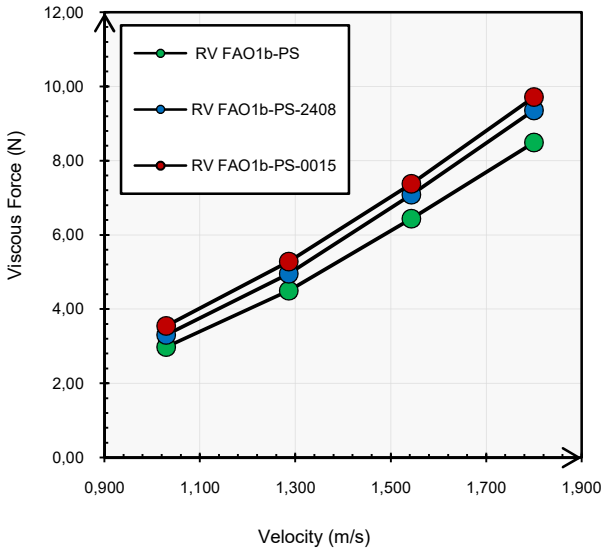

Figure 8: Viscous resistance

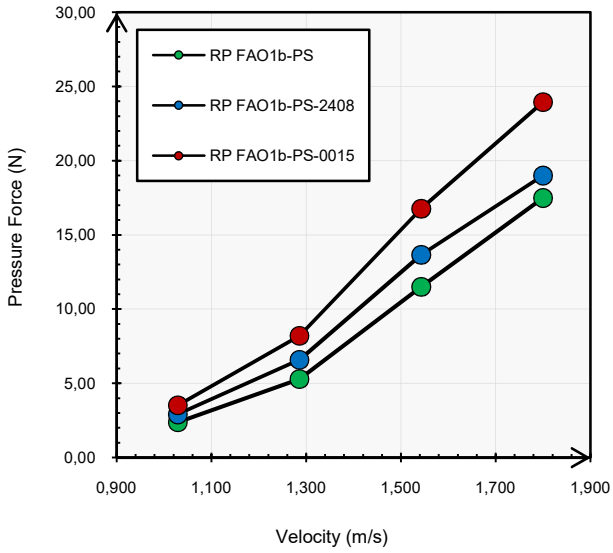

Figure 9: Pressure resistance

A more detailed examination reveals that the NACA 0015 configuration exhibits the most pronounced increase in viscous resistance among the tested variants. This phenomenon can be attributed to the foil's symmetrical cross-section, which promotes a nearly uniform pressure distribution on both sides. As a result, the configuration provides no significant hydrodynamic advantage for efficiently redirecting the local flow.

In contrast, the cambered geometry of the NACA 2408 profile facilitates smoother flow attachment along its contour by maintaining a more controlled and favourable pressure gradient. Consequently, although the NACA 2408 foil inherently adds to the total WSA, its optimized fluid structure interaction results in a comparatively smaller increment in frictional resistance than the symmetrical NACA 0015 profile.

4.3 Pressure Resistance

As illustrated in Figure 9, the pressure resistance across all three model variations exhibits a significant positive correlation with increased vessel velocity. In contrast to viscous resistance, which is primarily a function of hull surface friction, pressure resistance is governed by the pressure distribution surrounding the hull, wave-making phenomena, and flow separation effects. Throughout the evaluated velocity range, the baseline FAO1b-PS model consistently demonstrated the lowest pressure resistance values. Conversely the integration of a retractable bow foil resulted in elevated resistance levels, with the FAO1b-PS-0015 variant recording the highest pressure resistance, followed by the FAO1b-PS-2408.

These results suggest that the addition of a retractable bow foil does not facilitate wave attenuation or optimize pressure distribution; rather, it exacerbates the pressure differential between the fore and aft regions of the structural elements. The observed rise in pressure resistance is primarily driven by hydrodynamic imbalances generated by localized alterations in flow direction and fluid acceleration within the inflow region. These disturbances modify the incoming streamlines and interfere with the stability of the primary flow structure around the body. Consequently, the overall hydrodynamic resistance increases due to the combined effects of disturbed pressure distribution, intensified flow separation, altered boundary layer development, and reduced flow stability around the body.

A comparative evaluation between the two foil configurations reveals exactly how the geometric variations of the NACA profiles negatively impact the local pressure distribution. The FAO1b-PS-0015 model, utilizing a symmetrical NACA 0015 profile, generates a highly concentrated, severe high-pressure zone directly at its nose. This aggressive and blunt pressure spike correlates directly with the massive 27.48% resistance penalty observed in the quantitative data. Conversely, the FAO1b-PS-2408 model with its cambered profile induces an asymmetrical pressure gradient. While it still generates a problematic stagnation zone, its cambered nature slightly redistributes the frontal pressure, resulting in a relatively lower yet still significant15.23% penalty. In both cases, the presence of these massive pressure spikes at the bow forces the downstream fluid to negotiate strong adverse pressure gradients, thereby negatively impacting the boundary layer development along the rest of the wetted hull surface.

Ultimately, these visual pressure contour mappings provide the physical justification for the overall drag increments. The concentrated high-pressure zones on the frontal area of the foils clearly manifest as a severe form of interface resistance between the appendages and the bulbous bow. Instead of functioning as a drag-reduction mechanism, the physical blockage created by the retractable bow foils massively inflates the pressure resistance (form drag) component. This visual evidence clearly demonstrates that the combination of a dihedral bulbous bow and bow foils exacerbates all primary resistance components rather than optimizing them, establishing the baseline model as the most hydro dynamically efficient configuration.

JOMAse | Received: 05 March-2026 | Accepted: 30-March-2026 | [(70) 1: 64-71]
Published by International Society of Ocean, Mechanical and Aerospace Scientists and Engineers, www.isomase.org., ISSN: 2354-7065 & e-ISSN: 2527-6085

ISOMAse
International Society of Ocean, Mechanical and Aerospace Scientists and Engineers
Journal of Ocean, Mechanical and Aerospace
-Science and Engineering-
30 March 2026. Vol.70 No.1
DOI:
10.36842/jomase.v70i1.592

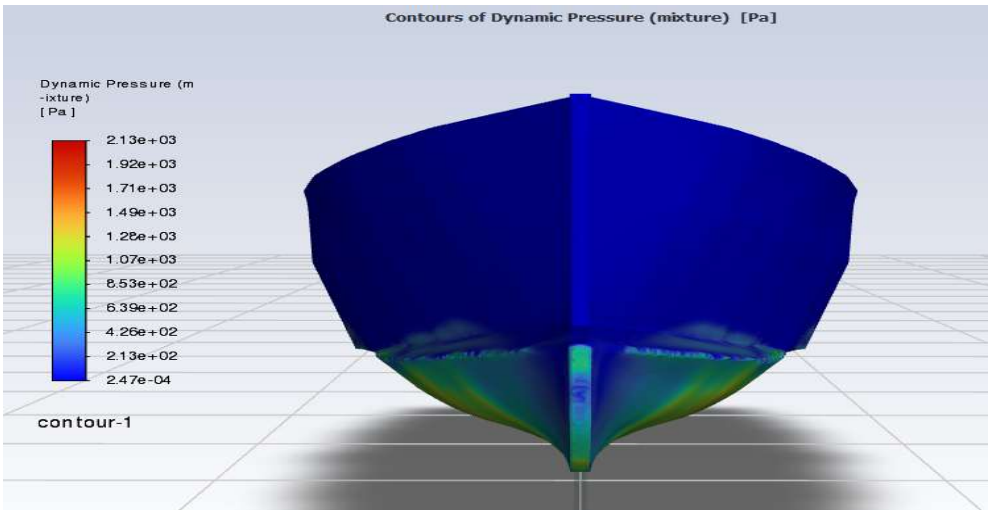

(a)

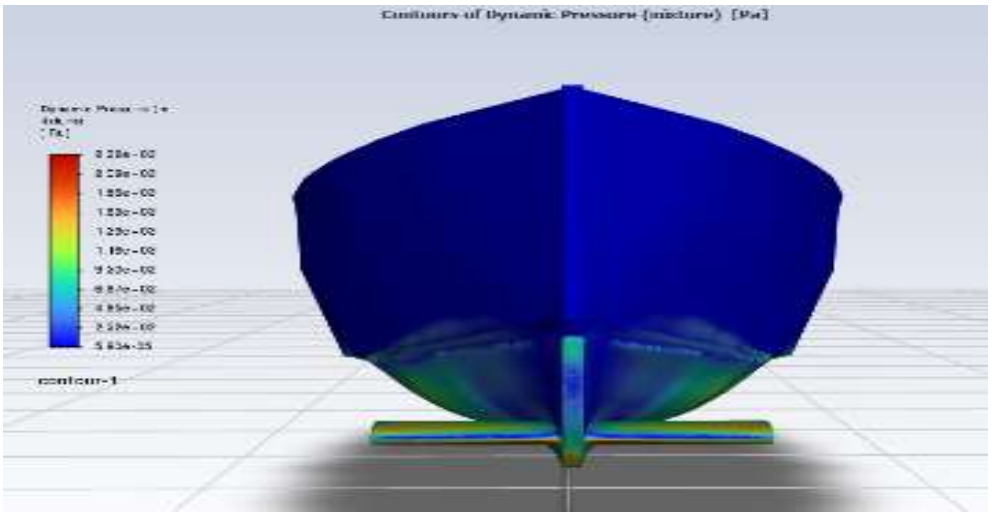

(b)

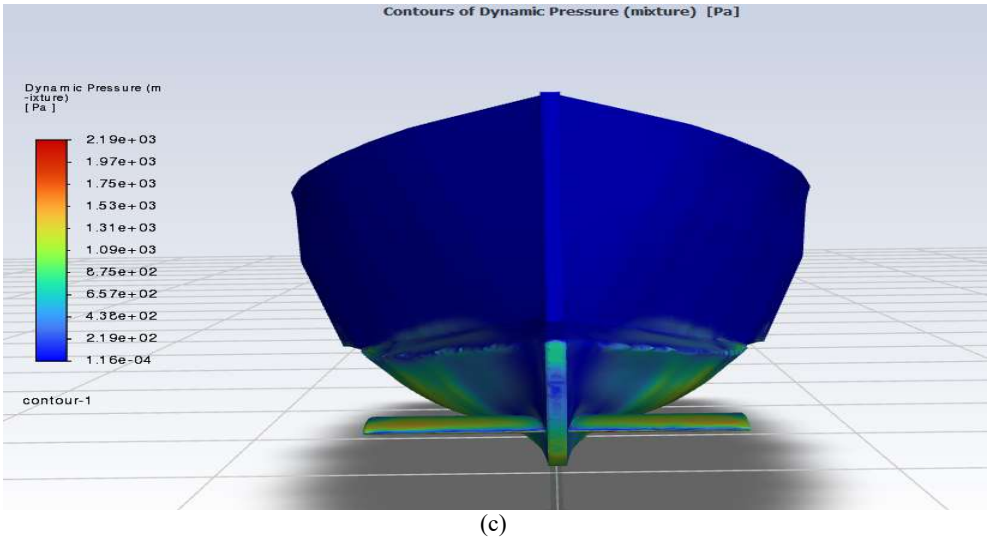

(c)

Figure 10: Comparison of dynamic pressure contours at the maximum velocity (1.8 m/s): (a) FAO1b-PS hull, (b) FAO1b-PS-0015, and (c) FAO1b-PS-2408

JOMAse | Received: 05 March-2026 | Accepted: 30-March-2026 | [(70) 1: 64-71]
Published by International Society of Ocean, Mechanical and Aerospace Scientists and Engineers, www.isomase.org., ISSN: 2354-7065 & e-ISSN: 2527-6085

5. CONCLUSION

Based on the CFD simulation results, the baseline FAO1b-PS model represents the most hydro dynamically efficient configuration, consistently producing the lowest total resistance across the entire investigated velocity range. At a reference velocity of 1,286 m/s, the total resistance for the FAO1b-PS model was recorded at 9.78 N, whereas the integration of retractable bow foils resulted in significant resistance penalties of 27.48% for the FAO1b-PS-0015 variant and 15.23% for the FAO1b-PS-2408 variant. These increments in total resistance are directly correlated with the expansion of the Wetted Surface Area (WSA) and the emergence of interface resistance, which disturbs the streamlined flow around the bulbous bow and inhibits the intended resistance reduction mechanisms. Furthermore, the observed upward trends in viscous resistance and pressure resistance with increasing velocity confirm that the geometric variations of the NACA 0015 and 2408 profiles negatively impact boundary layer development and pressure distribution. Consequently, the research objective of achieving a more than 10% reduction in total resistance was not realized, as the combination of a dihedral bulbous bow and retractable bow foils exacerbated all primary resistance components rather than optimizing them.

ACKNOWLEDGEMENTS

The authors would like to express their sincere gratitude to the Department of Naval Architecture, Faculty of Engineering, Universitas Pembangunan Nasional "Veteran" Jakarta, for providing the essential facilities and continuous academic support throughout the course of this research.

REFERENCES

[1] Suardi, S., Alamsyah, A.A., Nugraha, M. & Pawara, M.U. (2023). Experimental analysis of castor oil and diesel oil mixtures in a 4-stroke compression combustion engines. *International Journal of Mechanical Engineering Technologies and Applications*, 4(2), 167–176. doi: 10.21776/mechta.2023.004.02.6.

[2] Koričan, M., Perčić, M., Vladimir, N., Alujević, N. & Fan, A. (2022). Alternative Power Options for Improvement of the Environmental Friendliness of Fishing Trawlers. *Journal of Marine Science and Engineering*, 10(12).doi: 10.3390/jmse10121882.

[3] Regional Marine Pollution Emergency Response Centre for the Mediterranean Sea (REMPEC). (2020). *Annex VI Regulations for the Prevention of Air Pollution from Ships Regulation 1 Application*. https://marine21.marine.gov.my/appl/jict032008/jlsm/service/notice/MARPOL/annex6.pdf.

[4] Ali, M.A., Peng, H. & Qiu, W. (2019). Resistance prediction of two fishing vessel models based on RANS solutions. *Physics and Chemistry of the Earth*, 113, 115–122. doi: 10.1016/j.pce.2019.05.005.

[5] Lin, Y., He, J. & Li, K. (2018). Hull form design optimization of twin-skeg fishing vessel for minimum resistance based on surrogate model. *Advances in Engineering Software*, 123,38–50. doi: 10.1016/j.advengsoft.2018.05.010.

[6] Yu, J.W., Lee, M.K., Kim, Y.I., Suh, S.B. & Lee, I. (2021). An optimization study on the hull form and stern appendage for improving resistance performance of a coastal fishing vessel.*Applied Sciences (Switzerland)*, 11(13). doi: 10.3390/app11136124.

[7] Iqbal, M., Terziev, M., Tezdogan, T. & Incecik, A. (2025). Hull form optimisation to minimise the total resistance and dynamic responses of small fishing vessels. *Journal of Ocean Engineering and Technology*, 321. doi: 10.1016/j.oceaneng.2025.120357.

[8] Díaz-Ojeda H.R., Pérez-Arribas F. & Turnock S.R. (2023). The influence of dihedral bulbous bows on the resistance of small fishing vessels: A numerical study. *Journal of Ocean Engineering and Technology*, 281. doi: 10.1016/j.oceaneng.2023.114661.

[9] Bøckmann, E., Yrke, A. & Steen, S. (2018). Fuel savings for a general cargo ship employing retractable bow foils. *Applied Ocean Research*, 76, 1–10. doi: 10.1016/j.apor.2018.03.015.

[10] MollandA.F. & Turnock, S.R. (2007). Principles, data, design and applications. *Marine rudders and control surfaces.* doi: 10.1016/B978-0-7506-6944-3.X5000-8.

[11] Abbott, I.H. & Von Doenhoff, A.E. (1959). *Abbott, I.H. & Von Doenhoff, A.E. (1959). Theory of wing sections: Including a summary of airfoil data. Dover Publications.*

[12] Chrismianto, D., Yudo, H. & Rangga Dewa, N. (2020). Article ID: IJARET_11_04_007 Cite this Article: Deddy Chrismianto, Hartono Yudo, Kiryanto and Narendra Rangga Dewa, Modification of 30 Gt Fishing Vessels Using Hull Vane Naca 2408 Type for Reducing Ship Resistance. *International Journal of Advanced Research in Engineering and Technology (IJARET)*, 11(4), 57–62.

[13] Birk, L. (2019). *Fundamentals of Ship Hydrodynamics: Fluid Mechanics, Ship Resistance and Propulsion*: Wiley Liblary Online.

[14] Versteeg, H.K. & Malalasekera, W. (2007). *An Introduction to Computational Fluid Dynamics: The Finite Volume Method* (2nd ed.). Pearson Education.

[15] Menter, F. R., Kuntz, M. & Langtry, R. (2003). Two-equation eddy-viscosity turbulence models for engineering applications. *AIAA Journal*, 32(8), 1598–1605.

[16] Pérez-Arribas, F., Silva-Campillo, A. & Díaz-Ojeda, H.R. (2022). Design of dihedral bows: A new type of developable added bulbous bows-Experimental results. *Journal of Marine Science and Engineering*, 10(11), 1691. doi: 10.3390/jmse10111691.

[17] Food and Agriculture Organization (FAO). (2021). Report of the FAO Virtual Expert Workshop on the Toolbox for Fisheries Co-Management Evaluation. https://openknowledge.fao.org/items/ede3ac4a-c0e4-46ba-8465-168da649763f/full.

[18] Niklas, K. & Pruszko, H. (2023). The retrofitting of ships by applying retractable bow hydrofoils: A case study. *Journal of Ocean Engineering and Technology*, 9(4), 767–788. doi: 10.1007/s40722-023-00289-8.